Applied Energy 225 (2018) 27–41

Contents lists available at ScienceDirect

Applied Energy

journal homepage: www.elsevier.com/locate/apenergy

Estimating ramping requirements with solar-friendly flexible ramping product in multi-timescale power system operations

Mingjian Cui, Jie Zhang*

Department of Mechanical Engineering, The University of Texas at Dallas, Richardson, TX 75080, USA

HIGHLIGHTS

- A multi-timescale unit commitment and economic dispatch model is developed to estimate the ramping requirements.
- A solar power ramping product (SPRP) is developed and integrated into the multi-timescale dispatch model.
- A surrogate-based optimization model is developed to solve the ramping requirements problem.
- SPRP can reduce the total cost of flexible ramping reserves.

ARTICLE INFO

Keywords:
Economic dispatch
Latin hypercube sampling
Photovoltaic (PV)
Flexible ramping capability
Flexibility
Unit commitment

ABSTRACT

The increasing solar power penetration causes the need of additional flexibility for power system operations. Market-based flexible ramping services have been proposed in several balance authorities to address this issue. However, the ramping requirements in multi-timescale power system operations are not well defined and still challenging to be accurately estimated. To this end, this paper develops a multi-timescale unit commitment and economic dispatch model to estimate the ramping requirements. Furthermore, a solar power ramping product (SPRP) is developed and integrated into the multi-timescale dispatch model that considers new objective functions, ramping capacity limits, active power limits, and flexible ramping requirements. To find the optimal ramping requirement based on the level of uncertainty in netload, a surrogate-based optimization model is developed to approximate the objective function of the multi-timescale dispatch model that considers both economic and reliability benefits of the balancing authorities. Numerical simulations on a modified IEEE 118-bus system show that a better estimation of ramping requirements could enhance both the reliability and economic benefits of the system. The use of SPRP can reduce the flexible ramping reserves provided by conventional generators.

1. Introduction

Renewable energy is significantly impacting the economic and reliable operations of the power systems, especially with the rapid increase of renewable penetration [1–3]. As an important renewable source, solar power in the electric power grid rises continuously. Due to the effects of microclimates (e.g., solar irradiance, temperature, and passing clouds), solar power ramps occur frequently [4,5]. These solar power ramps, in addition to the uncertainty and variability of solar power, present new challenges to the balancing authorities. Multiple independent system operators (ISOs) have proposed a flexible ramping product to help improve the dispatch flexibility to integrate these variable and uncertain renewables such as wind and solar [6–8].

Recently, wind has been proposed to provide ramping service for the flexible operations of the power system [9–11], which also makes solar possible for balancing authorities to provide a solar-friendly ramping product in a similar manner. Solar power ramping product (SPRP) is essentially different from wind power ramping product (WPRP) that can be provided by any significant wind power ramp. SPRP should be provided by actual solar power ramp events (not due to diurnal pattern) that are caused by changes in short-term micro-climates. In addition, SPRP could potentially reduce the production cost by reducing the ramping reserve requirement provided by conventional thermal generators, and also possibly enhance the reliability of power system operations. Thus in this paper, we are exploring the capability of solar to provide such flexibility service, and also evaluating the values of solar-friendly flexible ramping product in terms of the reliability and economic benefits for power system operations [12,13].

* Corresponding author.
E-mail address: jiezhang@utdallas.edu (J. Zhang).

https://doi.org/10.1016/j.apenergy.2018.05.031
Received 11 November 2017; Received in revised form 30 March 2018; Accepted 5 May 2018

Nomenclature

Acronyms

SPRP	solar power ramping product
ISO	independent system operator
WPRP	wind power ramping product
MISO	midcontinent independent system operator
CAISO	California independent system operator
FESTIV	flexible energy scheduling tool for integration of variable generation
DU	day-ahead security-constrained unit commitment
RU	real-time security-constrained unit commitment
RE	real-time security-constrained economic dispatch
AGC	automatic generation control
OpSDA	optimized swinging door algorithm
FRP	flexible ramping product
MILP	mixed-integer linear programming
ACE	area control error
CPS2	control performance standard 2
NERC	North American electric reliability corporation
AACEE	absolute area control error in energy
KA	Kriging approximation
LHS	Latin hypercube sampling

Parameters

t,τ	indexes for time intervals
$T^{(\cdot)}$	number of time periods. $T^{\mathrm{RU}} = 4$ with 15-min time resolution in RU model and $T^{\mathrm{RE}} = 3$ with 5-min time resolution in RE model
NI	number of thermal units
NS	number of solar generators
NB	number of buses
$C_i^{t^{(\cdot)}}$	operation cost of thermal unit i during period t^{RU} and t^{RE}, in $
$S_i^{t^{(\cdot)}}$	start-up cost of thermal unit i during period t^{RU} and t^{RE}, in $
$\gamma_{i,t^{(\cdot)}}^{\mathrm{up}}$, $\gamma_{i,t^{(\cdot)}}^{\mathrm{dn}}$	bidding price of flexible up/down ramping reserves of thermal unit i during period t^{RU} and t^{RE}, in $/MWh
$p_s^{t^{(\cdot)}}$	power output of solar generator s at the end of period t^{RU} and t^{RE}, in MW
$P_i^{\min}$, $P_i^{\max}$	minimum/maximum generation of thermal unit i
$d_b^{t^{(\cdot)}}$	expected load of bus b at time $t^{(\cdot)}$, in MW
$\mathbf{PL}^{\max}$	vector of power limit for transmission lines
$\mathbf{D}$	vector of expected load or demand
$\mathbf{K_P}$, $\mathbf{K_S}$, $\mathbf{K_D}$	bus-thermal unit, bus-solar unit, and bus-load incidence matrices
$\mathbf{P}$, $\mathbf{P_S}$	vector of thermal dispatch and PV generation
$\mathbf{SF}$	shift factor matrix
$X_{i,\mathrm{on}}^{t^{(\cdot)}}$, $X_{i,\mathrm{off}}^{t^{(\cdot)}}$	ON/OFF time of thermal unit i at time $t^{(\cdot)}$
$T_{i,\mathrm{on}}$, $T_{i,\mathrm{off}}$	minimum ON/OFF time limits of unit i
R_i^{up}, R_i^{dn}	maximum up/down ramping rate of thermal unit i, in MW/min
L_C	a sufficient large constant
$UP_s^{t^{(\cdot)}}$, $DP_s^{t^{(\cdot)}}$	up/down solar power ramping product of solar generator s during period t^{RU} and t^{RE}, in MW
$URR_{t^{(\cdot)}}$	total flexible upward ramping reserve requirements during period t^{RU} and t^{RE}, in MW
$DRR_{t^{(\cdot)}}$	total flexible downward ramping reserve requirements during period t^{RU} and t^{RE}, in MW
m, n	index of time points in the solar power data
$R(\cdot)$	ramp rule for measured or forecasted solar power
$C(\cdot)$	natural ramp rule for the clear-sky solar power
$p_{\mathrm{C},s}^{t^{(\cdot)}}$	solar power generation in clear sky
p_t^{NL}	actual netload at time t
$\hat{p}_{t+5\mathrm{min}\mid t}^{\mathrm{NL}}$	forecasted netload for the next 5 min at time t
$\hat{p}_{t+15\mathrm{min}\mid t}^{\mathrm{NL}}$	forecasted netload for the next 15 min at time t
$\sigma_{t,5\mathrm{min}}$	standard deviation of netload in the RE model
$\sigma_{t,15\mathrm{min}}$	standard deviation of netload in the RU model
λ_e, λ_r	penalty multipliers for the economic and reliability benefits
$\underline{\alpha}$, $\overline{\alpha}$	minimum/maximum values of times of the standard deviation of netload in RE model
$\underline{\beta}$, $\overline{\beta}$	minimum/maximum values of times of the standard deviation of netload in RU model
x, μ_x, σ_x	variable to be normalized, its mean value, and standard deviation
$ACE_{t,inst}$	instantaneous ACE value at time period t
T_n, K_1, K_2	parameters used for the smoothed AGC mode
$\varphi_{(\cdot)}$	sensitivity coefficients
I_{RTD}, H_{RTD}	time resolution and horizon of the RE model
P_{WIND}, P_{LOAD}	amount of wind power and load on the system
P_{RAMP}	amount of total ramping available from the resources to manage the variability
T_{CPS2}	CPS2 interval, i.e., 10 min
$\mathbf{\Lambda}$	coefficient vector containing all the regression parameters and $\mathbf{\Lambda} = [\lambda_1,...,\lambda_6]^{\mathrm{T}}$
q, N_{S}	index and total number of sampled points (α_q, β_q)
$\lambda_{(\cdot)}$, θ, ω	parameters of the KA model
μ_α, μ_β	mean values of sampled α_q and β_q
σ_α, σ_β	standard deviations of sampled α_q and β_q

Variables and Functions

$p_i^{t^{(\cdot)}}$	dispatch of thermal unit i at the end of period t^{RU} and t^{RE}, in MW
$u_i^{t^{(\cdot)}}$	1 if unit i is scheduled on during period t^{RU} and t^{RE}; and 0 otherwise
$fu_i^{t^{(\cdot)}}$, $fd_i^{t^{(\cdot)}}$	scheduled flexible up/down ramping reserves of thermal unit i during period t^{DU}, t^{RU}, and t^{RE}, in MW
α, β	times of the standard deviation of netload in RU and RE models
α_{N}, β_{N}	normalized times of the standard deviation of netload in RU and RE models
$S_c(\cdot)$	positive score function used in the dynamic programming
$f(\cdot)$	multi-objective function for obtaining reliability benefits and minimizing dispatching cost
$\hat{f}(\alpha,\beta)$	Kriging approximation surrogate model
$f_E[\cdot]$	functional relationship between the economic metrics and times of standard deviation
$f_R[\cdot]$	functional relationship between the reliability metrics and times of standard deviation
$\mathscr{F}(\cdot)$	realization function of a regression model in KA
$\mathscr{R}(\cdot)$	correlation function in KA
$\mathbf{f}(\alpha,\beta)$	polynomial function vector set containing polynomials of orders 0, 1, and 2: $\mathbf{f}(\alpha,\beta) = [1,\alpha_{\mathrm{N}},\beta_{\mathrm{N}},\alpha_{\mathrm{N}}^2,\alpha_{\mathrm{N}}\beta_{\mathrm{N}},\beta_{\mathrm{N}}^2]$
$\nabla\hat{f}(\cdot)$	gradient matrix of KA
$H(\hat{f}(\cdot))$	Hessian matrix of KA
ρ	control factor used to limit the provision of SPRP
$p_{\mathrm{ESS}}^{t^{(\cdot)}}$	charged power of ESS at time $t^{(\cdot)}$

Currently, both the Midcontinent Independent System Operator (MISO) and California Independent System Operator (CAISO) have designed the ramping product to manage netload variations and uncertainties to maintain power balance in the real-time dispatch process [6,7,14]. Ramping products are defined at different real-time operation timescales, which should be secured five, ten, or fifteen minutes ahead based on the ISO's market rules. Both the 5-min and 10-min ahead ramping products can be sequentially integrated into the economic dispatch cycles run at a 5-min or 10-min time resolution. The 15-min ahead ramping products can be sequentially integrated into the real-time unit commitment cycles run at a 15-min time resolution. The market schemes and operation scales vary among different ISOs. A balance authority may only have 5-, 10-, or 15-min markets, but unlikely have all of them. In this paper, we only consider the 5- and 15-min ahead ramping products in the market scheme.

To effectively evaluate the impacts of solar power on the flexible ramping products, it is important to first accurately estimate the ramping requirements in power system operations. Currently, ramping requirements can be divided into soft and hard methods varying with the method of capturing the system-wide ramping capacity [15]. The soft method utilizes the demand curve to price the ramping capability violation and considers ramping requirements as decision variables added to both the objective function and constraints. The hard method considers ramping requirements as given values, based on the variability from the current dispatch interval to a future interval and the uncertainty at a future interval. MISO proposed a Gaussian-sigma rule based on the Gaussian distribution [7]. The ramping requirement was set as the netload variations plus the standard deviation of netload forecasting errors. Wang et al. [14] proposed a simulation-based method to determine the level of uncertainty in netload based on the MISO market rules from the perspective of reliability. To extend the work in [14], it would be interesting to optimally determine the level of uncertainty in netload by considering both the economic and reliability performance in power system operations. In addition, though multi-timescale power system operations have been progressed in recent years [11,16–18], few studies have focused on estimating ramping reserve requirements in a multiple timescales manner to ensure a realistic study.

Furthermore, the ramping requirement will be varying with the increase of solar power penetration. With the continuous improvement of solar forecasting accuracy, it is possible to use solar power to provide flexible ramping reserves in the future. Thus, it would also be interesting to study the impacts of solar-friendly flexible ramping product on estimating the ramping reserves provided by conventional thermal generators. To this end, this paper aims to design and integrate a solar power ramping product in multi-timescale power system operations, and to estimate the flexible ramping requirements by considering both the economic and reliability benefits in power system operations. The main innovations and contributions of this paper include: (i) developing a novel ramping requirements estimation method by using the surrogate-based optimization model; (ii) designing SPRPs by transforming negative characteristics of SPRPS into advantageous ones; and (iii) analyzing the impact of SPRPs on estimating ramping requirements of power system optimization models.

The organization of this paper is as follows. In Section 2, a modified multi-timescale scheduling model that considers the solar-friendly flexible ramping product and ramping requirement estimation is developed. Section 3 presents a developed surrogate-based optimization model to approximate the power system operations by simultaneously quantifying the economic and reliability metrics. Case studies and results analysis performed on a modified IEEE 118-bus system are discussed in Section 4. The controllability of SPRP is discussed in Section 5. Concluding remarks and future work are given in Section 6.

2. Multi-timescale scheduling models

To estimate the ramping requirement for power system operations, we use a multi-timescale scheduling method based on a simulation tool, Flexible Energy Scheduling Tool for Integration of Variable Generation (FESTIV) [16,19], as illustrated in Fig. 2. Four power system operation sub-models are included in FESTIV, including day-ahead security-constrained unit commitment (DU), real-time security-constrained unit commitment (RU), real-time security-constrained economic dispatch (RE), and automatic generation control (AGC), as shown in the left block of Fig. 2. The details of these sub-models are discussed in Sections 2.1 and 2.2. SPRP is designed and considered in each dispatch stage, which is integrated into FESTIV through a solar power ramp detection method, the optimized swinging door algorithm (OpSDA), as shown in the right block of Fig. 2. The details of OpSDA are discussed in Section 2.3. Ramping requirement estimation is discussed in Section 2.4.

The temporal coupling of sub-models is important because the configurable timing parameters will ensure a realistic study. Fig. 1 shows how the four sub-models are coupled with different timeframes. In this figure, I represents the interval length, t represents the time between updates, and H represents the scheduling horizon. For the DU sub-model, the interval resolution is I_{DU} (1 h). DU is simulated every t_{DU} (24 h) which is usually once per day in the current operation system. The optimization horizon (H_{DU}) in DU is 24 h (one day). The RU sub-model is repeated every t_{RU} (15 min) at an interval resolution of I_{RU} (15 min) and an optimization horizon of H_{RU} (45 min). The RE sub-model is repeated every t_{RE} (5 min) at an interval resolution of I_{RE} (5 min) and an optimization horizon of H_{RE} (10 min). The AGC sub-

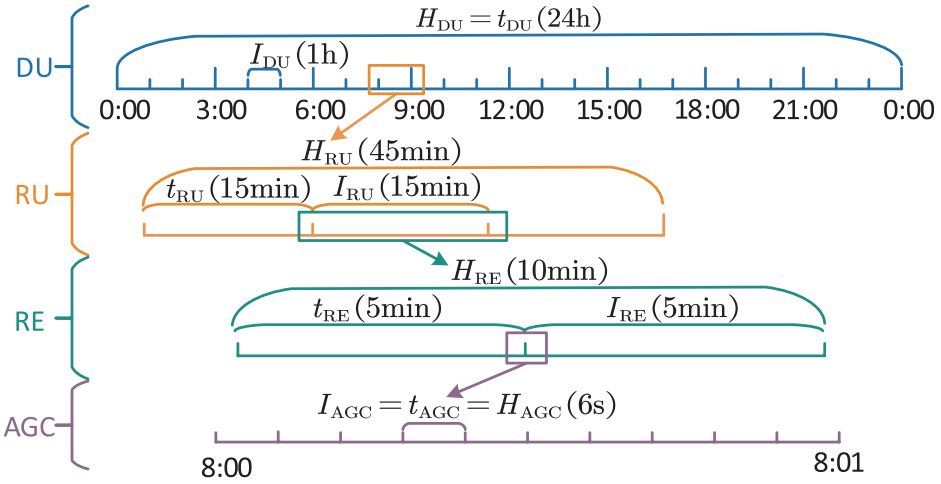

Fig. 1. Timeframes of FESTIV with four sub-models.

model is run every t_{AGC} (6 s). H_{AGC} and I_{AGC} are equal to t_{AGC}.

2.1. Objective functions

The objective functions and constraints of considering the flexible ramping products are adopted and modified from the CAISO's model. To address the flexibility challenge, CAISO has designed the flexible ramping products (FRPs) to reduce the frequency of power balance violations and created a ramp margin based on the forecasted ramping needs of adjacent intervals [6]. The bid costs of the flexible ramping reserves provided by thermal generators are defined same as that in the CAISO market. The objective function consists of the operation cost, start-up cost, and flexible ramping reserve cost. A piecewise linear approximation of the cost curves of generators is utilized to retain a mixed-integer linear programming (MILP) formulation. The objective function of DU and RU is given by:

$$\min \sum_{t^{(\cdot)}=1}^{T^{(\cdot)}} \left\{ \sum_{i=1}^{NI} [\underbrace{C_i^{t^{(\cdot)}}(p_i^{t^{(\cdot)}}, u_i^{t^{(\cdot)}}) + S_i^{t^{(\cdot)}}(u_i^{t^{(\cdot)}}, u_i^{t^{(\cdot)}-1})}_{\text{Operation and Start-up Cost}} + \underbrace{\gamma_{i,t^{(\cdot)}}^{\text{up}} fu_i^{t^{(\cdot)}} + \gamma_{i,t^{(\cdot)}}^{\text{dn}} fd_i^{t^{(\cdot)}}}_{\text{Ramping Reserve Cost}}] \right\} \tag{1}$$

where $t^{(\cdot)}$ is $t^{60\text{min}}$ or $t^{15\text{min}}$ in the DU or RU models, respectively. The objective function of RE is stated as:

$$\min \sum_{t^{5\text{min}}=1}^{T^{5\text{min}}} \left\{ \sum_{i=1}^{NI} [\underbrace{C_i^{t^{5\text{min}}}(p_i^{t^{5\text{min}}})}_{\text{Operation Cost}} + \underbrace{\gamma_{i,t^{5\text{min}}}^{\text{up}} fu_i^{t^{5\text{min}}} + \gamma_{i,t^{5\text{min}}}^{\text{dn}} fd_i^{t^{5\text{min}}}}_{\text{Ramping Reserve Cost}}] \right\} \tag{2}$$

where the generator status is obtained through the RU model.

2.2. Equality and inequality constraints

The objective functions in the FESTIV-OpSDA model comply with a number of prevailing constraints, including the system load balance in (3), DC transmission capacity limits in (4), minimum on/off time limits in (5) and (6), max/min capacity limits of thermal units in (7), up- and down-ramping rate limits in (8) and (9), max/min active power limits in (10) and (11), up- and down-ramping reserve limits in (12) and (13), up- and down-ramping reserve requirements in (14) and (15), and SPRP estimation in (16) and (17). Similarly to [14], other types of ancillary services (regulation, spinning, non-spinning, and replacement reserves) are not considered in this paper in view of their different purposes and deployment procedures. For the sake of simplicity, $t^{(\cdot)}$ represents $t^{5\text{min}}$, $t^{15\text{min}}$, and $t^{60\text{min}}$ in the following formulations. Prevailing RU and RE models share similar non-integer constraints. Note that the binary variables $u_i^{t^{5\text{min}}}$ and $u_i^{t^{5\text{min}}-1}$ have been determined in the RU sub-model and used as a constant in the RE sub-model. The main modifications include active power limits, ramping capacity limits, and flexible ramping requirements Eqs. (10)–(15). More detailed information about how to design the system ramping requirement constraints can be found in [6,11,20].

Each unit is subject to its own operating constraints, including minimum up and down time constraints, ramping rate constraints, and initial condition constraints. This paper aims to develop and integrate the flexible ramping reserves into FESTIV. In the objective functions in (1) and (2), the flexible up- and down-ramping reserve costs are calculated by the expressions $\gamma_{i,t^{(\cdot)}}^{\text{up}} fu_i$ and $\gamma_{i,t^{(\cdot)}}^{\text{dn}} fd_i$, respectively. Based on the proposed solar ramping product concept that each unit must provide both up- and down-ramping reserves, the sum of the power output (p_i) and the prepared up-ramping reserve (fu_i) of each unit must not exceed its capacity ($P_i^{\max}$) in (10). Similarly, the power output (p_i) of each unit must be capable of providing the down-ramping reserve (fd_i) but not lower than its minimum generation ($P_i^{\min}$) in (11). The upward ramping capability limit in (12) ensures that each unit's up-ramping reserve (fu_i) does not exceed its maximum up-ramping rate (R_i^{up}) over the market clearing interval ($\triangle t^{(\cdot)}$). Similarly, the downward ramping capability limit in (13) ensures that each unit's down-ramping reserve (fd_i) does not exceed its maximum down-ramping rate (R_i^{dn}) over the market clearing interval ($\triangle t^{(\cdot)}$). The upward flexible ramping requirement in (14) ensures that the total amount of upward flexible ramping reserve ($\sum_{i=1}^{NI} fu_i^{t^{(\cdot)}}$) provided by thermal units and upward SPRP ($\sum_{s=1}^{NS} UP_s^{t^{(\cdot)}}$) provided by solar generators meets the upward ramping requirement ($URR_{t^{(\cdot)}}$). The downward flexible ramping requirement in (15) ensures that the total amount of downward flexible ramping reserve ($\sum_{i=1}^{NI} fd_i^{t^{(\cdot)}}$) provided by thermal units and downward SPRP ($\sum_{s=1}^{NS} DP_s^{t^{(\cdot)}}$) provided by solar generators meets the downward ramping requirement ($DRR_{t^{(\cdot)}}$). The design of SPRP is similar with that of wind power ramping product based on our previous research in [11,21]. More detailed information will be introduced in Section 2.3. In time intervals of SPRPs (ξ), the upward SPRP (UP_s) is designed in (16) when the solar power ramping rate is positive; otherwise, the upward SPRP equals 0. In time intervals of SPRPs (ξ), the downward SPRP (DP_s) is designed in (17) when the solar power ramping rate is negative; otherwise, the downward SPRP equals 0. It is assumed that the maximum available solar ramping is fully used to provide the ramping reserve requirements. These solar ramping products are prioritized to provide ramping services. The SPRP is far from sufficient for providing all the required ramping services. Hence, instead of controlling the provision of SPRP, which can limit the use of SPRP, we seek to take full advantage of entire SPRPs to decrease the ramping reserves provided by thermal generators.

$$\sum_{i=1}^{NI} p_i^{t^{(\cdot)}} + \sum_{s=1}^{NS} p_s^{t^{(\cdot)}} = \sum_{b=1}^{NB} d_b^{t^{(\cdot)}} \tag{3}$$

$$-\mathbf{PL}^{\max} \leqslant \mathbf{SF} \times [\mathbf{K_P} \times \mathbf{P} + \mathbf{K_S} \times \mathbf{P_S} - \mathbf{K_D} \times \mathbf{D}] \leqslant \mathbf{PL}^{\max} \tag{4}$$

$$[X_{i,\text{on}}^{t^{(\cdot)}-1} - T_{i,\text{on}}] \cdot [u_i^{t^{(\cdot)}-1} - u_i^{t^{(\cdot)}}] \geqslant 0 \tag{5}$$

$$[X_{i,\text{off}}^{t^{(\cdot)}-1} - T_{i,\text{off}}] \cdot [u_i^{t^{(\cdot)}} - u_i^{t^{(\cdot)}-1}] \geqslant 0 \tag{6}$$

$$P_i^{\min} \times u_i^{t^{(\cdot)}} \leqslant p_i^{t^{(\cdot)}} \leqslant P_i^{\max} \times u_i^{t^{(\cdot)}}, \quad \forall\, i, \forall\, t^{(\cdot)} \tag{7}$$

$$p_i^{t^{(\cdot)}} - p_i^{t^{(\cdot)}-1} \leqslant R_i^{\text{up}} \times \triangle t^{(\cdot)} + L_C \times (2 - u_i^{t^{(\cdot)}} - u_i^{t^{(\cdot)}-1}) \tag{8}$$

$$p_i^{t^{(\cdot)}-1} - p_i^{t^{(\cdot)}} \leqslant R_i^{\text{dn}} \times \triangle t^{(\cdot)} + L_C \times (2 - u_i^{t^{(\cdot)}} - u_i^{t^{(\cdot)}-1}) \tag{9}$$

$$p_i^{t^{(\cdot)}} + fu_i^{t^{(\cdot)}} \leqslant P_i^{\max} \times u_i^{t^{(\cdot)}}, \quad \forall\, i, \forall\, t^{(\cdot)} \tag{10}$$

$$p_i^{t^{(\cdot)}} - fd_i^{t^{(\cdot)}} \geqslant P_i^{\min} \times u_i^{t^{(\cdot)}}, \quad \forall\, i, \forall\, t^{(\cdot)} \tag{11}$$

$$fu_i^{t^{(\cdot)}} \leqslant R_i^{\text{up}} \times \triangle t^{(\cdot)}, \quad \forall\, i, \forall\, t^{(\cdot)} \tag{12}$$

$$fd_i^{t^{(\cdot)}} \leqslant R_i^{\text{dn}} \times \triangle t^{(\cdot)}, \quad \forall\, i, \forall\, t^{(\cdot)} \tag{13}$$

$$\sum_{i=1}^{NI} fu_i^{t^{(\cdot)}} + \underbrace{\sum_{s=1}^{NS} UP_s^{t^{(\cdot)}}}_{\text{SPRP}} \geqslant URR_{t^{(\cdot)}}, \quad \forall\, i, \forall\, t^{(\cdot)} \tag{14}$$

$$\sum_{i=1}^{NI} fd_i^{t^{(\cdot)}} + \underbrace{\sum_{s=1}^{NS} DP_s^{t^{(\cdot)}}}_{\text{SPRP}} \geqslant DRR_{t^{(\cdot)}}, \quad \forall\, i, \forall\, t^{(\cdot)} \tag{15}$$

$$UP_s^{t^{(\cdot)}} = \begin{cases} \max\{[p_s^{t^{(\cdot)}+\Delta t^{(\cdot)}} - p_s^{t^{(\cdot)}}], 0\}, & t^{(\cdot)} \in \xi \\ 0, & t^{(\cdot)} \in \overline{\xi} \end{cases} \tag{16}$$

$$DP_s^{t^{(\cdot)}} = \begin{cases} \max\{[p_s^{t^{(\cdot)}} - p_s^{t^{(\cdot)}+\Delta t^{(\cdot)}}], 0\}, & t^{(\cdot)} \in \xi \\ 0, & t^{(\cdot)} \in \overline{\xi} \end{cases} \tag{17}$$

2.3. Solar power ramping products detected by dynamic programming

Ramps in solar power consist of natural ramps and actual ramp events. The distinctions between natural ramps and actual ramp events can be explained from two perspectives: physical phenomenon and power system operations. From the perspective of physical phenomenon, natural ramps is expected to occur in both the actual solar power generation and the clear-sky power generation. The occurrence of natural ramps is due to the diurnal pattern of solar radiation. Actual ramp events (not due to diurnal pattern) are caused by changes in short-term micro-climates, such as passing clouds [22]. From the perspective of power system operations, both natural and actual solar ramps can be managed by the flexible ramping reserve provided by thermal units. This concept has been designed by both MISO and CAISO [6,7,14]. However, the actual ramp events can be additionally used in this paper to take advantage of their negative characteristics, i.e., large fluctuations (significant increase or decrease) of solar power in a short time period. Hence, the negative characteristic of actual solar power ramp events can be transformed into an advantageous one as the SPRP. Under this circumstance, this paper assumes that only actual solar power ramp events provide SPRP. Note that using natural ramps to provide SPRP is beyond the scope of this paper, which can be studied in the future. In the current market, the ramping product can only be represented by generation output difference between two successive time intervals. While in our developed ramping product model, SPRPs are provided in the time intervals when the upward and downward solar power ramp events occur (rather than successive time intervals). This model has been successfully used for the design of wind power ramping product, more detailed information on which can be found in [11,21].

Hence, SPRPs are defined as those ramp events that occur in the actual solar power generation however not in the clear-sky power generation. After identifying all significant ramps in the measured or forecasted solar power generation, the clear-sky solar ramps are removed as natural ramps that are caused by the diurnal pattern of solar radiation. First, the solar power data is segregated by the OpSDA [23] with a predefined compression deviation ε. Then all extracted segments are input into the dynamic programming (the light blue block in Fig. 2) and merged to yield a set of SPRPs. Designed as positive characteristics of solar power ramps, the SPRP is integrated into the multi-timescale dispatch model that considers new objective functions, ramping capacity limits, active power limits, and flexible ramping requirements. A positive score function S_c is used in the dynamic programming to detect all SPRPs, given by:

$$S_c(m,n) = (m-n)^2 \times [1-C(m,n)] \times R(m,n) \tag{18}$$

$$R(m,n) = \begin{cases} 1, & \text{if } |p_s^m - p_s^n| > 0.15 \text{ p.u.} \\ 0, & \text{if } |p_s^m - p_s^n| \leqslant 0.15 \text{ p.u.} \end{cases} \tag{19}$$

$$C(m,n) = \begin{cases} 1, & \text{if } |p_{C,s}^m - p_{C,s}^n| > 0.15 \text{ p.u.} \\ 0, & \text{if } |p_{C,s}^m - p_{C,s}^n| \leqslant 0.15 \text{ p.u.} \end{cases} \tag{20}$$

where $R(m,n) = 1$ when a ramp occurs in the measured or forecasted solar power. $C(m,n) = 1$ when a natural ramp occurs in the clear-sky generation. Both $R(m,n)$ and $C(m,n)$ are defined as the change in solar power magnitude without the ramping duration limit [23–25].

In this paper, the change in solar power output is set to be greater than 15% of the installed capacity of solar generators (i.e., 0.15 p.u.). Due to the diurnal pattern of solar power, the aim of (18) is to assure the design of a true SPRP. The OpSDA combines the adjacent segments in the same direction and detects SPRPs by removing those occurring in the clear-sky power generation. A more detailed description of OpSDA can be found in [22,23].

As shown in Fig. 3, the natural upward ramp spans from 8:00 to 10:00 and the natural downward ramp spans from 15:00 to 17:00. These two natural ramps occur due to the diurnal pattern of solar radiation and are not used to design the SPRP. In order to transform a negative characteristic of solar power ramp event into an advantageous one, the upward ramp event spanning from 13:00 to 14:00 and the downward ramp event spanning from 14:00 to 14:30 are used to design the SPRP in this paper. Differently with thermal units, solar power can only provide SPRPs when actual ramps occur. Taking the time interval spanning from 10:00 to 13:00 as an example, the slight solar power generation output difference (sometimes even approximately equal 0) in successive time intervals could not be used to provide a satisfactory amount of SPRPs.

2.4. Ramping reserve requirement estimation

Different methodologies have been used to define the ramping reserve requirements. For example, MISO designs the ramping reserve requirements by assuming that the uncertain netload follows a Gaussian distribution and utilizes the level of uncertainty based on a Gaussian-sigma rule, where the uncertainty is represented by the standard deviation of the netload [7]. The netload is defined as the load demand minus the renewable energy sources from solar power [7,14,26,27]. For the RE model, the amount of upward ramping reserve requirement URR_t^{RE} is set as the variation between the forecasted netload $\hat{p}_{t+5\mathrm{min}|t}^{\mathrm{NL}}$ and the actual netload p_t^{NL} plus 'α' times of the standard deviation [14], given by:

$$URR_t^{\mathrm{RE}} = \max\{0, \hat{p}_{t+5\mathrm{min}|t}^{\mathrm{NL}} - p_t^{\mathrm{NL}} + \alpha\sigma_{t,5\mathrm{min}}\} \tag{21}$$

Symmetrically, the amount of downward ramping reserve

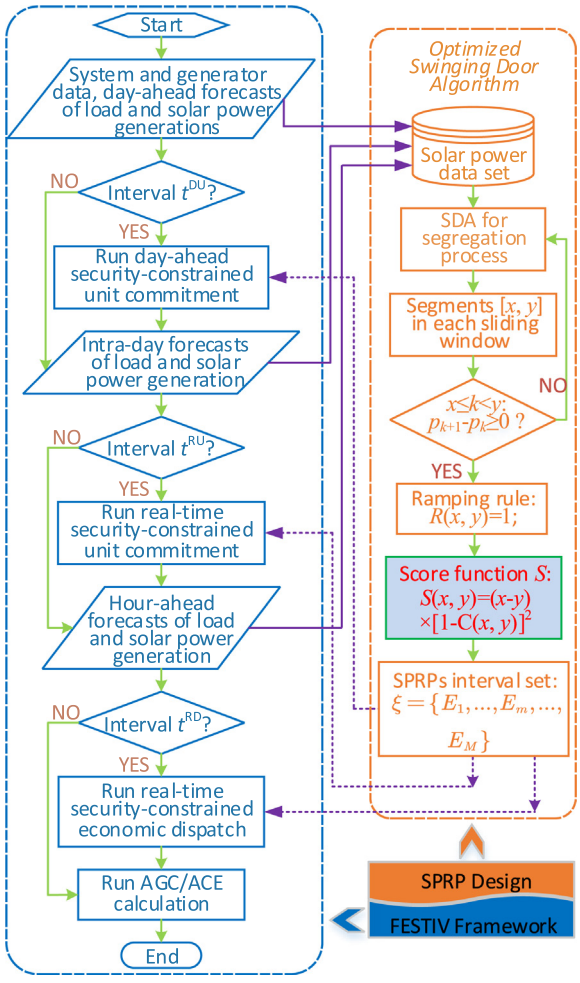

Fig. 2. Multi-timescale scheduling model based on FESTIV and OpSDA.

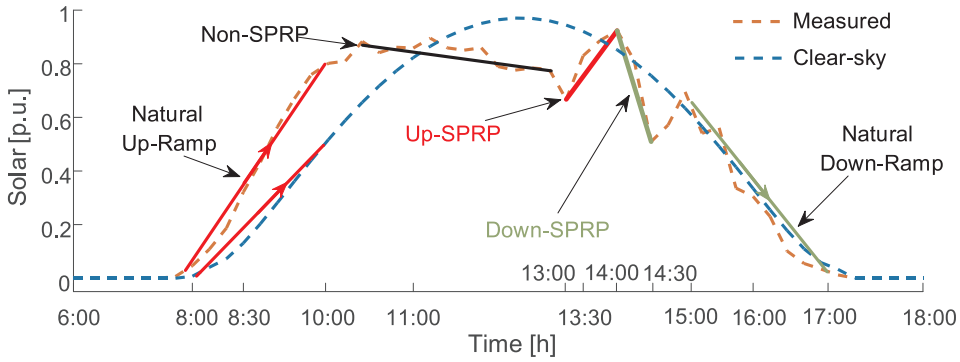

Fig. 3. An example of solar power ramping product in one day.

requirement DRR_t^{RE} is set as the variation between the forecasted netload $\hat{p}_{t+5min|t}^{NL}$ and the actual netload p_t^{NL} minus 'α' times of the standard deviation, given by:

$$DRR_t^{RE} = \max\{0, p_t^{NL} - \hat{p}_{t+5min|t}^{NL} + \alpha\sigma_{t,5min}\} \quad (22)$$

In this paper, we also utilize the ramping reserve requirement defined in the RE model and further extend it to the RU model. Similarly, the amount of upward ramping reserve requirement URR_t^{RU} in RU is set as the variation between the forecasted netload $\hat{p}_{t+15min|t}^{NL}$ and the actual netload p_t^{NL} plus 'β' times of the standard deviation:

$$URR_t^{RU} = \max\{0, \hat{p}_{t+15min|t}^{NL} - p_t^{NL} + \beta\sigma_{t,15min}\} \quad (23)$$

where $\sigma_{t,15min}$ is approximated by the total probability theory as $\sigma_{t,15min} = \sqrt{3}\sigma_{t,5min}$ for Gaussian distribution [28].

Symmetrically, the amount of downward ramping reserve requirement DRR_t^{RU} in RU is set as the variation between the forecasted netload $\hat{p}_{t+15min|t}^{NL}$ and the actual netload p_t^{NL} minus 'β' times of the standard deviation, given by:

$$DRR_t^{RU} = \max\{0, p_t^{NL} - \hat{p}_{t+15min|t}^{NL} + \beta\sigma_{t,15min}\} \quad (24)$$

By optimally determining the values of α and β, the ramping requirements of both RE and RU models can hence be estimated with the consideration of both economic and reliability benefits. Thus, a multi-objective optimization model is developed, where both economic and reliability metrics ($f_E[\cdot]$ and $f_R[\cdot]$) are represented as functions of the multipliers of standard deviations, i.e., α and β. However, these functions cannot be analytically expressed due to the complexity of power system operations. Thus in this paper, a surrogate model is developed to approximate the multi-timescale power system scheduling models, which is described in Section 3. In addition, most of current literatures only consider the economic benefits by minimizing the total dispatching cost in the RE timescale. The multi-objective function developed in this paper also minimizes the system's area control error (ACE) to obtain the reliability benefits in both RE and RU timescales, given by:

$$\min f(\alpha,\beta) = \lambda_e \cdot f_E[RR_{t,5min}^{RE}(\alpha), RR_{t,15min}^{RU}(\beta)] + \lambda_r \cdot f_R[RR_{t,5min}^{RE}(\alpha), RR_{t,15min}^{RU}(\beta)], \quad \underline{\alpha} \leqslant \alpha \leqslant \overline{\alpha}, \ \underline{\beta} \leqslant \beta \leqslant \overline{\beta} \quad (25)$$

where the initial ranges of α and β are determined by heuristics as $[\underline{\alpha}, \overline{\alpha}]$ and $[\underline{\beta}, \overline{\beta}]$, respectively [14]. λ_e and λ_r are penalty multipliers that can be selected based on the preference of balancing authorities. $f_E[\cdot]$ represents the functional relationship between the economic metrics and (α, β). $f_R[\cdot]$ represents the functional relationship between the reliability metrics and (α, β). A detailed description of economic and reliability metrics is provided in the following section. Due to the scale difference, both the economic and reliability metrics are normalized as follows:

$$x_N = (x - \mu_x)/\sigma_x \quad (26)$$

where x is the variable to be normalized. μ_x and σ_x are the mean value and standard deviation of multiple samples, respectively.

2.5. Economic and reliability metrics

The total power system production cost is directly computed by the FESTIV-OpSDA model. The cost of each generator to supply energy at every AGC interval for the entire study period is calculated. This includes the start-up, no-load, and incremental energy cost, as well as any bid in flexible ramping reserve costs. The economic profit is the revenue minus the total cost of all generation resources. The revenue is the total revenue of all generation resources in the system after getting paid the locational marginal price for energy and any ancillary service price for ancillary service provisions.

Reliability metrics are calculated based on the system's ACE and the Control Performance Standard 2 (CPS2) proposed by the North American Electric Reliability Corporation (NERC) [29,30]. ACE is the difference between the sum of total generation and load at any time, which is the main driver of all imbalance metrics, give by:

$$ACE_t = K_1 ACE_{t,inst} + \frac{K_2}{T_n}\int_{t-T_n}^{t} ACE_{\tau,inst}\, d\tau \quad (27)$$

where ACE_t is the smoothed ACE value of the system at time period t. $ACE_{t,inst}$ represents the instantaneous ACE value at time period t. The term τ is the index for time intervals. The terms T_n, K_1, and K_2 are parameters used for the smoothed AGC mode.

Absolute area control error in energy (AACEE) is the absolute value of ACE at every t_{AGC} interval, where t_{AGC} is the highest time resolution (in seconds) at which AGC is run. AACEE is a function of the time resolution of the RE (I_{RTD}), the time horizon of the RE (H_{RTD}), the amount of wind power on the system (P_{WIND}), the load (P_{LOAD}), and the amount of total ramping available from the resources to manage the variability (P_{RAMP}), formulated as:

$$AACEE = \varphi_1 I_{RTD} + \varphi_2 H_{RTD} + \varphi_3 P_{WIND} + \varphi_4 P_{LOAD} + \varphi_5 P_{RAMP} \quad (28)$$

where φ is the sensitivity coefficient and can be calculated from the standard deviation of output changes at different timescales, i.e., $\varphi_1 = \partial AACEE/\partial I_{RTD}$; $\varphi_2 = \partial AACEE/\partial H_{RTD}$; $\varphi_3 = \partial AACEE/\partial P_{WIND}$; $\varphi_4 = \partial AACEE/\partial P_{LOAD}$; and $\varphi_5 = \partial AACEE/\partial P_{RAMP}$.

CPS2 is a NERC reliability standard that measures the amount of intervals where the absolute value of ACE exceeds a predefined threshold [31]. Based on CPS2, the reliability indicator ACE_{CPS2} measures the sum of instantaneous ACE until the 10-min CPS2 interval (L10) ends. Thus, the unit of ACE_{CPS2} is MW-10 min and the τth ACE_{CPS2} is formulated as:

$$ACE_{CPS2,\tau} = \sum_{t=(\tau-1)\times T_{CPS2}\times 60}^{\tau\times T_{CPS2}\times 60 - t_{AGC}} ACE_{t,inst} \times \frac{t_{AGC}}{60 T_{CPS2}} \quad (29)$$

where T_{CPS2} is the CPS2 interval, i.e., 10 min. τ is the index of the τth ACE_{CPS2} value.

Overall, it should be noted that lower ACE, AACEE, and ACE_{CPS2}

indicate a better reliability performance. These metrics have been widely used in literature for the analysis of power system operations. Ela and O'Malley [16] calculated these reliability metrics to analyze the uncertainty impacts of wind power forecast errors. Ela et al. [32] also analyzed the impacts of the netload variability with wind integration based on these reliability metrics calculated by ACE. Wang et al. [33] measured the reliability improvements by calculating ACE for improved wind power forecasting. Cui et al. [11] found that the reliability of power system operations was enhanced with wind power ramping products by calculating ACE and corresponding reliability metrics.

3. Surrogate-based optimization

3.1. Surrogate model of multi-objective function

The Kriging surrogate model has been widely used in design and optimization community [34–37]. It is used to provide approximations of computationally expensive simulations and experiments. For example, Huang et al. [34] developed a design optimization method based on the Kriging surrogate model for the shape optimization of an aeroengine turbine disc. Song et al. [35] developed a Kriging surrogate model to design and optimize a plate-fin-type heat sink. Gao et al. [36] used a Kriging surrogate model to identify the optimal tip locations of an internal crack in cantilever plates. Xia et al. [37] employed the Kriging surrogate model in the finite element analysis to reduce the computing time for multi-objective robust optimization of electromagnetic devices. The optimization problems in power system operations are complex and generally computationally expensive, especially for the multiple timescales power system operations studied in this paper. Surrogate modeling such as Kriging is expected to reduce the computational burden significantly. In this paper, the ramping reserve requirements estimation problem makes it possible to use the Kriging surrogate model for an optimal solution.

First, the economic and reliability metrics are calculated through multi-timescale power system operations (e.g., FESTIV-OpSDA), which generally cannot be represented by straightforward mathematical functions of "α" and "β" that determine the ramping requirements. Thus, to successfully integrate the multi-objective function in (25) into the overall optimization problem, an approximation model needs to be developed. To this end, surrogate modeling that is widely used in the multidisciplinary design optimization society [38], is adopted here to approximate the $f(\alpha,\beta)$ in (25) by replacing the complex power system operation simulations. Then, the optimization can be performed directly based on the surrogate model. In this paper, a Kriging surrogate model is developed to approximate the objective f in (25) as a function of ramping requirement design variables, α and β. A design and analysis of computer experiments [39] is performed based on the FESTIV-OpSDA platform. The Kriging approximation (KA) surrogate model, $\hat{f}(\alpha,\beta)$, is established to formulate the deterministic response $f(\alpha,\beta)$ in (25) with a two dimensional input, given by:

$$\hat{f}(\alpha,\beta) = \mathscr{F}(\lambda;\alpha,\beta) + \mathscr{R}(\omega;\alpha,\beta) \approx f(\alpha,\beta) \quad \underline{\alpha} \leqslant \alpha \leqslant \overline{\alpha},\ \underline{\beta} \leqslant \beta \leqslant \overline{\beta} \tag{30}$$

where $\mathscr{F}$ is a realization function of a regression model, given by:

$$\mathscr{F}(\lambda;\alpha,\beta) = \mathbf{f}(\alpha,\beta)\Lambda \tag{31}$$

where $\mathbf{f}(\alpha,\beta)$ is a function vector set containing polynomials of orders 0, 1, and 2, i.e., $\mathbf{f}(\alpha,\beta) = [1,\alpha_N,\beta_N,\alpha_N^2,\alpha_N\beta_N,\beta_N^2]$. The variables α_N and β_N represent the normalization of variables α and β, respectively, i.e., $\alpha_N = (\alpha-\mu_\alpha)/\sigma_\alpha$ and $\beta_N = (\beta-\mu_\beta)/\sigma_\beta$. The coefficient vector Λ contains all the regression parameters, i.e., $\Lambda = [\lambda_1,\ldots,\lambda_6]^T$. $\mathscr{R}$ is a correlation function, given by:

$$\mathscr{R}(\theta,\omega;\alpha,\beta) = \sum_{q=1}^{N_S} \omega_q e^{-[\theta_\alpha(\alpha-\alpha_q)^2/\sigma_\alpha^2+\theta_\beta(\beta-\beta_q)^2/\sigma_\beta^2]} \tag{32}$$

where (α_q, β_q) is sampled by the Latin hypercube sampling (LHS) [40] and used to simulate the objective $f(\alpha_q,\beta_q)$ in (25) using the FESTIV-OpSDA model. The total number of sampled points (α_q, β_q) is N_S. The mean values of (α_q, β_q) are expressed as $\mu_\alpha = \frac{1}{N_S}\sum_{q=1}^{N_S}\alpha_q$ and $\mu_\beta = \frac{1}{N_S}\sum_{q=1}^{N_S}\beta_q$. The standard deviations of (α_q, β_q) are expressed as

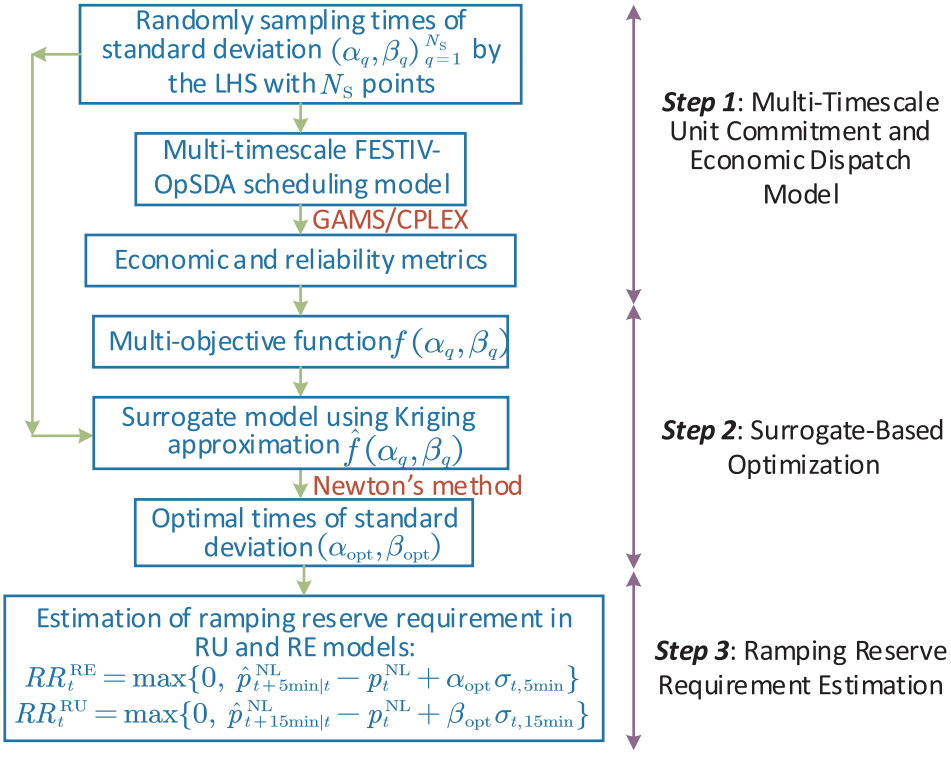

Fig. 4. The flow chart of estimating ramping reserve requirements by using the surrogate-based optimization.

$\sigma_\alpha = \sqrt{\frac{1}{N_S}\sum_{q=1}^{N_S}(\alpha_q - \mu_\alpha)^2}$ and $\sigma_\beta = \sqrt{\frac{1}{N_S}\sum_{q=1}^{N_S}(\beta_q - \mu_\beta)^2}$. All the parameters of the KA model ($\mathbf{\Lambda}$, θ, and ω) are calculated by the generalized least squares estimate [41]. The optimization of the surrogate model (30) is solved by using the Newton's method. The gradient, $\nabla\hat{f}(\alpha,\beta)$, and Hessian matrix, $H(\hat{f}(\alpha,\beta))$, of the KA model are deduced in Appendix A, respectively.

3.2. Procedure of estimating ramping reserve requirements

The flow chart of estimating ramping reserve requirements by using the surrogate-based modeling is shown in Fig. 4, which consists of three major steps: multi-timescale unit commitment and economic dispatch models, surrogate-based optimization, and ramping reserve requirement estimation. The three major steps are described as follows:

- ***Step 1***: Randomly sample times of standard deviation $(\alpha_q,\beta_q)_{q=1}^{N_S}$ by using LHS with N_S points. The corresponding ramping reserve requirements are determined by these samples (as described in Section 2.4), and input into the multi-timescale FESTIV-OpSDA scheduling model (as described in Sections 2.1,2.3). Both economic and reliability metrics are then calculated, as described in Section 2.5.
- ***Step 2***: The multi-objective function $f(\alpha,\beta)$ that is calculated by the economic and reliability metrics, and the sampled times of standard deviation (α,β) are approximated by the surrogate-based optimization model, as described in Section 3.1. Then, the optimal $(\alpha_{opt},\beta_{opt})$ is solved by the Newton's method based on the gradient and Hessian matrix.
- ***Step 3***: The estimated ramping reserve requirements are finally determined by the variation between the forecasted and actual netload plus 'α_{opt}' or 'β_{opt}' times of the standard deviation.

4. Case studies and results

4.1. Test cases

We perform numerical simulations on a modified IEEE 118-bus system using the FESTIV-OpSDA platform. All tests are carried out by using the General Algebraic Modeling System (GAMS) Distribution 24.7 [42], and solved using ILOG CPLEX 12.6 [43] on two Intel-e5-2603 1.6-GHz workstations with 32 GB of RAM memory. This system has 54 thermal units, 186 branches, and 91 load buses. The parameters of generators, transmission network, and load profiles are given in [44,45]. The system peak demand is 4,064 MW at the time stamp 18:46:24. To present a more realistic renewable-based generation system, the IEEE 118-bus system (as shown in Fig. 5) is modified by allocating 10 solar generators with the same location in [11], based on the apparent power of the loads and the distance of transmission lines. More detailed information about the allocation of solar generators can be found in [33]. These 10 solar generators are integrated into three zones: (i) Bus 4, 26, and 27 in the top left zone; (ii) Bus 40, 49, and 62 in the top right zone; and (iii) Bus 89, 100, 107, and 112 in the bottom right zone. SPRP is used to analyze the results of Sections 4.2, 4.3 and 4.4. Section 4.5 compares the results with and without SPRP. Section 4.6 compares the results with and without confidence levels.

Solar power data is collected from the Watt-sun forecasts [46]. Watt-sun solar forecasting is developed based on a situation-dependent multi-expert machine learning method, which combines the linear model, random forests, and support vector machine methods to enhance the forecast accuracy. It leans on historical forecasts. A dozen of single machine-learning models are set-up and ingest the multiple numerical weather prediction models for the situation dependent learning. The algorithm that provides the best accuracy for the last two days is selected for future solar power forecasts. Numerical results have shown an approximately 30% improvement in solar irradiance/power forecasting accuracy compared to forecasts based on the best individual method. Detailed information on the Watt-sun solar forecasting system

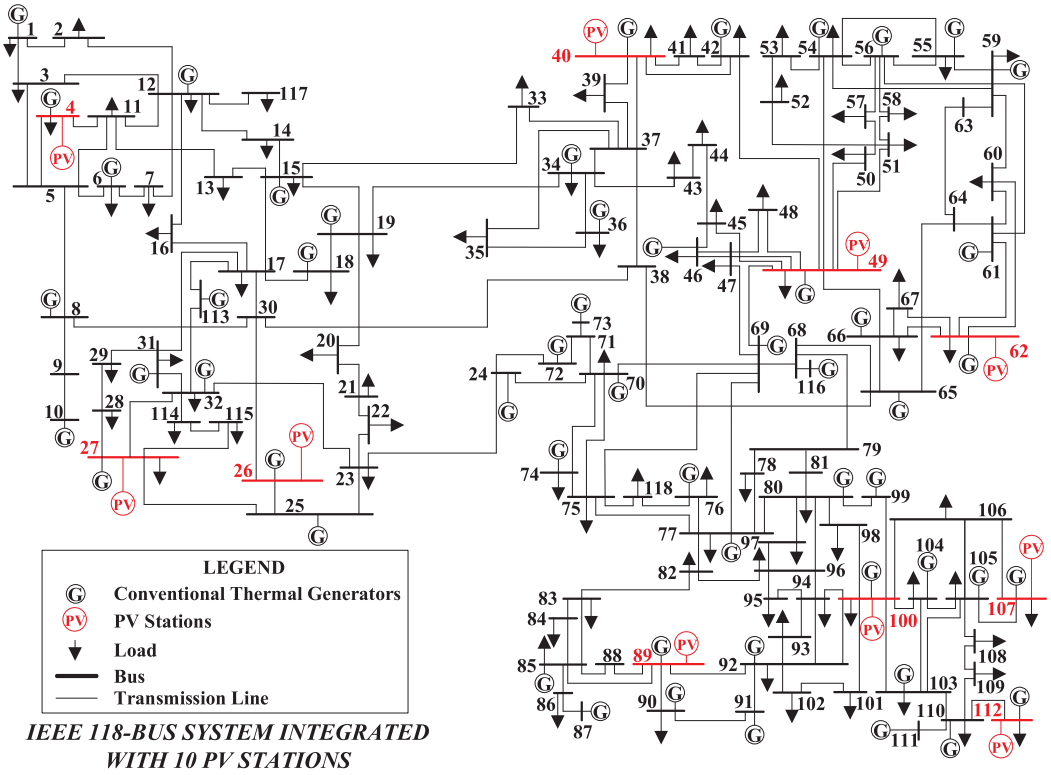

Fig. 5. The modified IEEE 118-bus system with 10 solar generators.

can be found in [46].

Clear sky is a hypothetical field assuming no clouds. Clear-sky solar power generation means the solar power generation that is directly converted from solar irradiance in this hypothetical clear-sky field. The solar irradiance data are collected from the Solar Resource & Meteorological Assessment Project (SOLRMAP) developed by the National Renewable Energy Laboratory (NREL) [47]. Then the solar power data is calculated through the collected solar irradiance data by using the PV_LIB toolbox [48].

4.2. Simulation results

Fig. 6 shows the performance of the KA surrogate model and the convergence history of obtaining the optimal multipliers of the standard deviation in the modified IEEE 118-bus system. The approximated KA model and corresponding MSEs are illustrated in Fig. 6(a) and (b), respectively. The estimated parameters of this surrogate model are listed in Table 1 with a same penalty multiplier, $\lambda_e = \lambda_r = 0.5$. The iterative process using the Newton's method with multiple contours is shown in Fig. 6(c). It is shown that the optimal solution of the surrogate-based optimization is obtained at the point $\alpha_{min} = 0.69$ and $\beta_{min} = 1.26$. The optimization convergence history of multiple simulations using the LHS sampling method is shown in Fig. 6(d). It is observed that the optimal results are robust with respect to different LHS samples. To validate the accuracy of the surrogate-based optimization results, a Monte-Carlo simulation is performed using the LHS sampling method with 10,000 runs, as shown in Fig. 7. The mean values of α_{opt} and β_{opt} are normally distributed around 0.69 and 1.26 with relatively small standard deviations 0.0163 and 0.0149, respectively.

Table 1
Parameters of the KA model with penalty multipliers of $\lambda_e = \lambda_r = 0.5$.

λ_1	λ_2	λ_3	λ_4	λ_5	λ_6	θ_α	θ_β
−0.865	0.692	0.011	0.294	−0.013	0.632	1.250	1.249
ω_1	ω_2	ω_3	ω_4	ω_5	ω_6	ω_7	ω_8
0.351	0.057	1.501	0.495	0.167	−0.729	−0.189	−0.482
ω_9	ω_{10}	ω_{11}	ω_{12}	ω_{13}	ω_{14}	ω_{15}	ω_{16}
−0.851	0.206	1.476	−0.881	−0.498	−0.111	−0.721	0.229
ω_{17}	ω_{18}	ω_{19}	ω_{20}	ω_{21}	ω_{22}	ω_{23}	ω_{24}
−1.633	0.009	1.089	−0.741	0.072	4.267	0.967	6.223
ω_{25}	ω_{26}	ω_{27}	ω_{28}	ω_{29}	ω_{30}		
−5.911	−5.728	0.646	0.638	0.381	−0.303		

The optimal results with different numbers of samples of α and β are illustrated in Fig. 8. It is seen when the number of samples is 22, we can get a relatively convergent optimum with and $\beta_{opt} \approx 1.26$. It means that the total execution time could be approximatively reduced from 15 h with 30 points to 11 h with 22 points (about 30 min for one sample) with a satisfactory precision.

The results of ramping reserves provided by thermal units are compared in Fig. 9. Fig. 9a compares the estimated up- and down-ramping reserves provided by thermal units in RU and RE models. The total energy of up- and down-ramping reserves provided by thermal units in the RE model is 251 MWh, and the total energy of up- and down-ramping reserves provided by thermal units in the RU model is 538 MWh. It is observed that the RE model requires less ramping

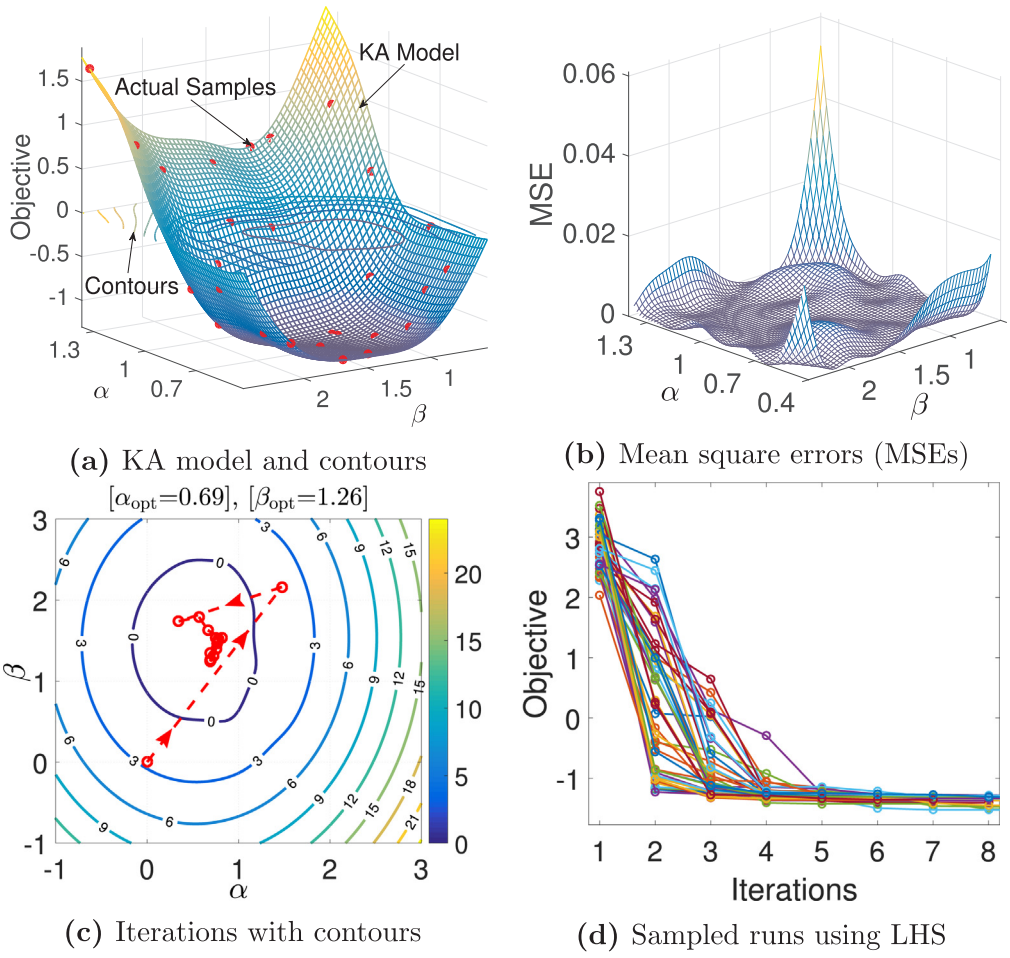

(a) KA model and contours (b) Mean square errors (MSEs)

(c) Iterations with contours (d) Sampled runs using LHS

Fig. 6. Performance of the KA model and the convergence history of obtaining the optimal multipliers of the standard deviations using the Newton's method.

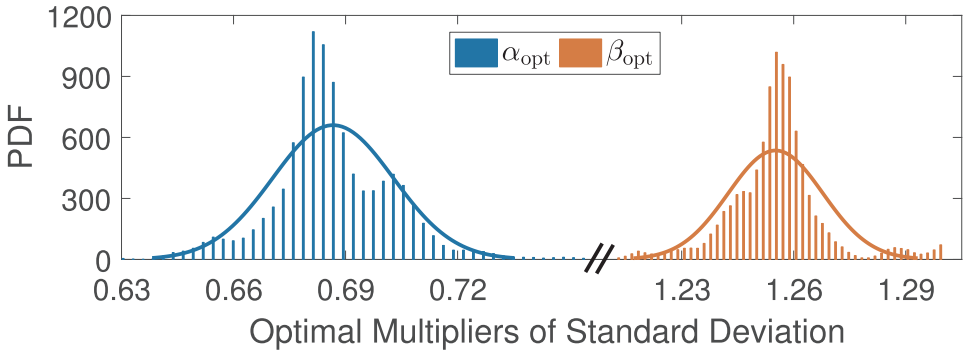

Fig. 7. Optimal multipliers values of the standard deviation using the LHS method based on statistical analysis with 10,000 simulation runs. The mean values of α_{min} and β_{min} are 0.69 and 1.26, respectively, and the standard deviations are 0.0163 and 0.0149, respectively.

reserves from thermal units than the RU model. This is mainly because the netload variation in RE (5-min time resolution) is less than that in RU (15-min time resolution). Fig. 9b compares the total estimated ramping reserves provided by thermal units with SPRP (the red line) and without SPRP (the blue line), which are 2431 MW × 5 min and 2523 MW × 5 min, respectively. In this case, SPRP saves approximately 3.63% [=(2523 − 2431)/2523] of ramping reserves provided by thermal units. When the solar power penetration level increases, this saving percentage is expected to increase accordingly.

To study the sensitivity of ramping reserves to the solar power forecasting accuracy, solar power data with a small forecasting error interval from 6 MW to 6 MW is simulated. Fig. 10 shows how the solar power forecasting accuracy impacts the total ramping reserves of the power system. The solar power forecasts are generated using a predefined normally distributed error that is randomly added to the perfect solar power forecast. The measured solar power which is called the perfect solar forecast is taken as the 100% accuracy. Based on the 100% accurate solar power, forecast errors are uniformly increased by a percentage (20%) to create other decreased forecasting accuracy scenarios (i.e., 80%, 60%, 40%, 20%, and 0%). Probability distribution functions (PDFs) of forecasting errors are shown in Fig. 10a. b shows that total ramping reserves of the system in different forecasting cases are generally not sufficiently scheduled compared to the perfect forecasting case (100%), since SPRPs are overestimated by forecasts.

4.3. Accuracy validation of the surrogate-based optimization

Fig. 11 compares the optimization results with different penalty multipliers. It is observed that when reliability benefits are preferred over economic benefits, i.e., $\lambda_r < \lambda_e$ in Case *c*3, both optimal α and β coefficients are increased in RE and RU models, compared to Case *c*2 when $\lambda_r = \lambda_e$. It results in more ramping requirements scheduled according to (21) and (23) to obtain more reliability benefits. When economic benefits are preferred over reliability benefits, i.e., $\lambda_e < \lambda_r$ in Case *c*1, both α and β coefficients are decreased, compared to Case *c*2 when $\lambda_r = \lambda_e$. Under this circumstance, less ramping reserve is scheduled according to (21) and (23) to obtain more economic benefits. Thus, the ramping requirements estimation accurately reflects the preference of balancing authorities.

Table 2 compares the economic and reliability benefits by randomly using two sets of α and β values to the optimal solution with the same penalty multiplier: $\lambda_e = \lambda_r = 0.5$, where all the metrics are normalized by (26). The optimal values of $\alpha_{opt} = 0.69$ and $\beta_{opt} = 1.26$ generate the minimum multi-objective value, −1.305, comparing to other α and β values. The increase of β in RU model significantly impacts economic metrics comparing to reliability metrics, as shown in the left half of Table 2. This is because reliability metrics are calculated at the AGC timescale (6-s time resolution) from which the RU timescale (15-min time resolution) difference is longer than the RE timescale (5-min time resolution). In the right half of Table 2, the increase of α significantly impacts both economic and reliability metrics. When α increases from 0.19 to 0.69, the economic metric increases by 12.62%, however the reliability metric decreases by 902.78%. The final aggregated multil-objective reaches to the minimum, −1.305.

4.4. Comparison of different standard deviations using the estimated ramping reserve requirements

Table 3 compares the reliability and economic metrics by randomly choosing standard deviation values with the optimal coefficients: $\alpha = 0.69$ and $\beta = 1.26$ in Section 4.2. Smaller AACEE and σ_{ACE} indicate a better performance in terms of the reliability indicators. A higher profit and lower cost indicate a better performance in terms of the economic indicators. It is shown that both AACEE and σ_{ACE} increase with the

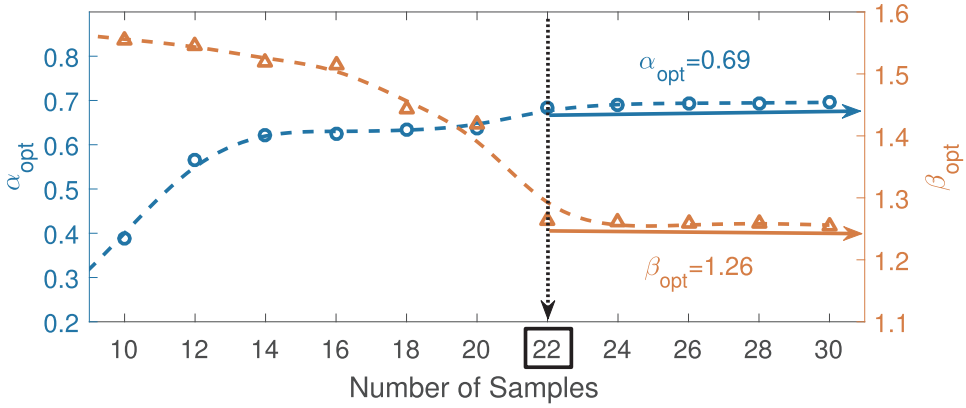

Fig. 8. Optimal results with different number of training points of α and β.

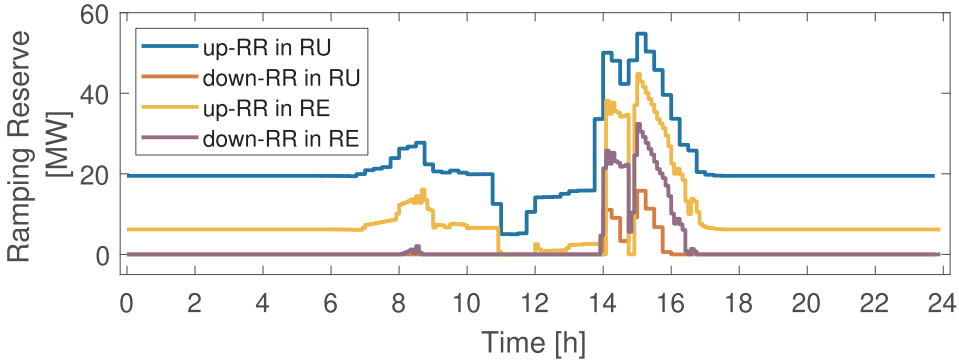

(a) Estimated ramping reserves provided by thermal units.

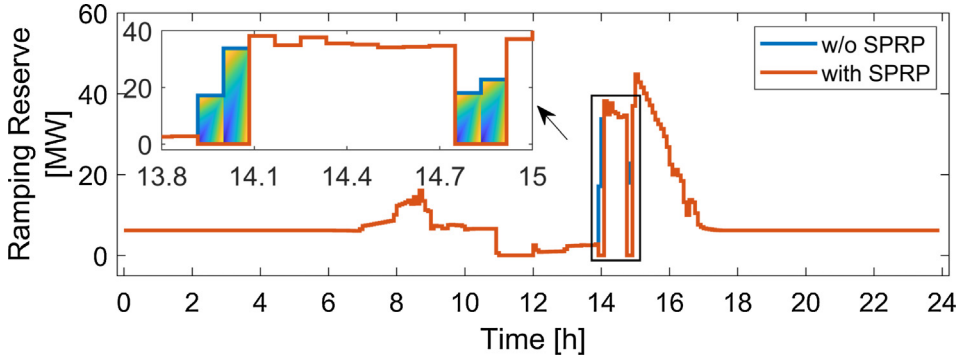

(b) Estimated ramping reserves provided by thermal units with and without SPRP.

Fig. 9. Comparison of estimated ramping reserves provided by thermal units.

standard deviation of netload. However, the economic benefits do not significantly change with the level of uncertainty in netload (i.e., the standard deviation value). This is because the total amount of netload does not significantly change, which makes the total power system production cost relatively constant with a slight decrease. Consequently, the system obtains a slight increase of the profit. Fig. 12 compares the reliability metrics to show the curves of ACE_{CPS2} and ACE. The curve of ACE_{CPS2} shows slight fluctuations with the increase of standard deviation of netload. The curve of ACE significantly increases with the standard deviation of netload, which results in the increase of the absolute ACE (AACEE) and the standard deviation of ACE (σ_{ACE}).

4.5. Different penalty multipliers with and without SPRP

Table 4 compares the optimal coefficients of the multi-objective function in (25). Two cases with SPRP and without SPRP are compared in this table. Similarly to Fig. 11, both α_{opt} and β_{opt} are increased with the preference of reliability benefits, no matter considering SPRP or not. The β_{opt} value is significantly reduced when using SPRP to provide ramping services, which means SPRP may play an important role in designing ramping requirements for the RU model at a 15-min timescale.

In order to separately analyze the impacts of SPRP on both the economic and reliability benefits, an indicator, $I_{(\cdot)}$, is developed by using the multi-objective function with SPRP (Mul_S) and without SPRP ($\overline{Mul_S}$), given by:

$$I_{(\cdot)} = \sum |Mul_S| - \sum |\overline{Mul_S}| \tag{33}$$

When the economic benefits are preferred (i.e., $\lambda_e < \lambda_r$), the indicator is $I_{\lambda_e < \lambda_r} = 0.236$. When the reliability benefits are preferred (i.e., $\lambda_e > \lambda_r$), the indicator is $I_{\lambda_e > \lambda_r} = 1.978$. Since $I_{\lambda_e > \lambda_r} > I_{\lambda_e < \lambda_r}$, SPRP would likely contribute more to the reliability benefits than to the economic benefits in power system operations. This finding can be used to estimate ramping reserve requirements. With the consensus that both the reliability and economic benefits are important to the system, the penalty multiplier λ_e of economic benefits in (25) is suggested to be slightly smaller than the penalty multiplier λ_r of reliability benefits (i.e., $\lambda_e < \lambda_r$).

4.6. Results comparison with and without confidence levels

To improve the performance of the developed model, the two-sigma rule is used to ensure that the realized confidence level is larger than 95%. Here the realized confidence level is defined as the ratio of successful simulation runs to the total simulation runs (10,000). A successful simulation run means a simulation scenario with load successfully satisfied by the generation. According to the two-sigma rule [49], a confidence level larger than 95% requires that the values of both α and β (i.e., times of 'sigma') should respectively be greater than 2. Under this circumstance, two cases are performed. In the first case, the 95% confidence level is not considered, which means the values of both α and β are not constrained by the two-sigma rule, i.e., $0 \leqslant \alpha \leqslant +\infty$ and $0 \leqslant \beta \leqslant +\infty$. In the second case, the 95% confidence level is strictly required, which means the values of both α and β must be constrained by the two-sigma rule, i.e., $2 \leqslant \alpha \leqslant +\infty$ and $2 \leqslant \beta \leqslant +\infty$.

Table 5 compares the results of estimated ramping reserve requirements with and without considering confidence levels. For the RE sub-model, the optimal times of standard deviation α_{opt} increase from 0.69 to 2.11, when confidence levels are considered. The realized confidence level increases from 50.98% to 96.52%. For the RU sub-model, the optimal times of standard deviation β_{opt} increase from 1.26 to 2.44, when confidence levels are considered. The realized confidence level increases from 79.24% to 98.54%. The optimal variables α_{opt} and β_{opt} need to be increased to obtain the higher realized confidence levels.

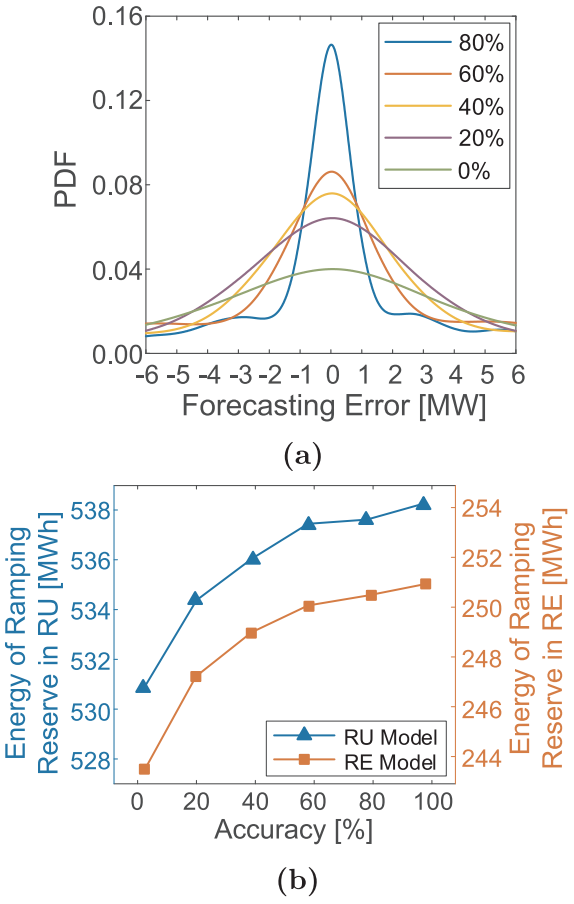

Fig. 10. Sensitivity of total ramping reserves to solar power forecasting accuracy.

Hence, the ramping requirements also increase with more production costs, approximately \$0.42 M (=1.48 − 1.06).

5. Discussion on the controllability of SPRP

With the increasing penetration of solar power in future power grid, SPRP is expected to save more ramping reserves provided by thermal units. If SPRP can provide more ramping reserves than the ramping reserve requirement, power system operators need to control the priority of SPRP for supplying ramping reserves. Taking the upward ramping reserve in (14) as an example, there are two strategies that can be used to control the ramping reserve provided by SPRP. The first strategy is to set a control factor, ρ, for SPRP based on the operation experience of power system operators. The control factor ρ is used to limit the provision of SPRP. Under this strategy, the constraint in (14) can be modified as:

$$\sum_{i=1}^{NI} fu_i^{t^{(\cdot)}} + \rho \cdot \underbrace{\sum_{s=1}^{NS} UP_s^{t^{(\cdot)}}}_{\text{SPRP}} \geqslant URR_{t^{(\cdot)}}, \quad \forall\, i\,, \forall\, t^{(\cdot)}, 0 < \rho < 1 \tag{34}$$

The modified constraint (34) indicates that only $\rho \times 100\%$ of the whole SPRP can be used to provide ramping reserves. The control factor ρ is defined by power system operators.

The second strategy is to install energy storage systems (ESS) to absorb the redundant upward SPRP. If SPRP can provide more ramping reserves than the ramping reserve requirement, the ESS can be charged to control the combined ramping reserves of SPRP and ESS, i.e., $p_{\text{Comb}}^{t^{(\cdot)}} = \sum_{s=1}^{NS} UP_s^{t^{(\cdot)}} - p_{\text{ESS}}^{t^{(\cdot)}}$. Under this strategy, the constraint in (14) can be modified as:

Table 2
Comparisons of different α and β to the benchmark optimal solution with penalty multipliers of $\lambda_e = \lambda_r = 0.5$.

$\alpha_{\text{opt}} = 0.69$				$\beta_{\text{opt}} = 1.26$			
β	Eco.	Rel.	Mul.	α	Eco.	Rel.	Mul.
0.66	2.189	−1.155	0.516	0.19	0.832	0.144	0.488
1.26	0.937	−1.156	−1.305	0.69	0.937	−1.156	−1.305
1.86	0.971	−1.156	−0.092	1.19	0.889	−0.937	−0.024

Table 3
Metrics at different standard deviation values using the optimal coefficients: $\alpha = 0.69$, $\beta = 1.26$.

Standard deviation	Reliability metrics		Economic metrics	
	AACEE [MWh]	σ_{ACE} [MW]	Total cost [\$M]	Total profit [\$M]
0.23%	429.41	40.93	1.0601	14.866
0.30%	433.73	41.21	1.0600	14.873
0.38%	436.42	41.53	1.0599	14.875

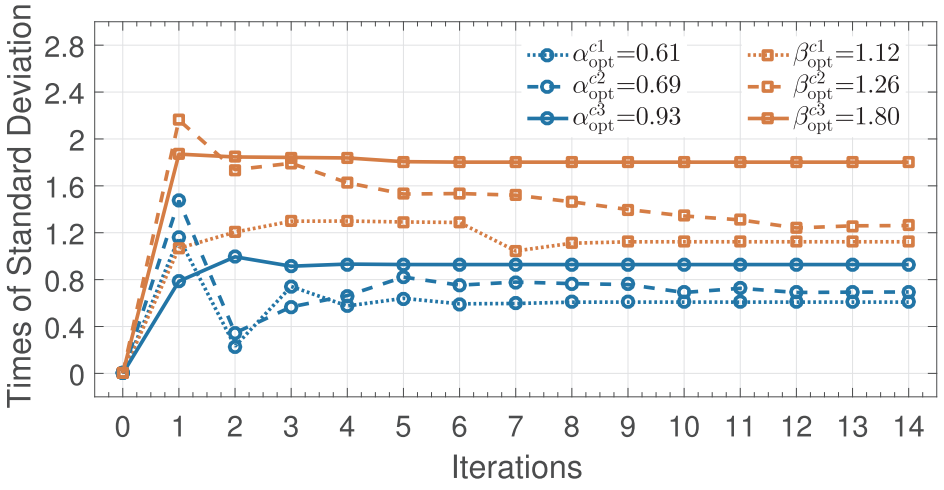

Fig. 11. Optimization convergence histories of three Cases. The terms 'c1', 'c2', and 'c3' represent simulation cases with different penalty multipliers: (λ_e, λ_r) = (0.2, 0.8), (0.5, 0.5), and (0.8, 0.2), respectively.

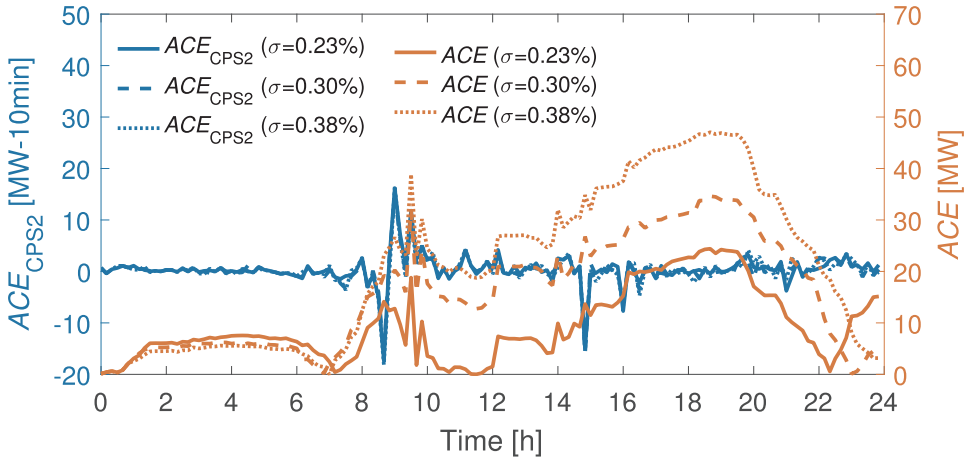

Fig. 12. Comparison of reliability impacts for different standard deviation values (σ).

Table 4
Optimal coefficients considering different penalty multipliers with SPRP and without SPRP.

(λ_e, λ_r)	With SPRP			W/o SPRP		
	α_{opt}	β_{opt}	Mul.	α_{opt}	β_{opt}	Mul.
(0.1, 0.9)	0.604	1.008	−2.415	0.9019	2.471	−2.078
(0.2, 0.8)	0.608	1.123	−2.123	0.9020	2.481	−2.054
(0.3, 0.7)	0.613	1.173	−1.839	0.9022	2.491	−2.033
(0.4, 0.6)	0.621	1.211	−1.566	0.9024	2.502	−2.014
(0.5, 0.5)	0.694	1.261	−1.305	0.9026	2.513	−1.997
(0.6, 0.4)	0.856	1.353	−1.278	0.9030	2.526	−1.983
(0.7, 0.3)	0.916	1.792	−1.413	0.9031	2.541	−1.973
(0.8, 0.2)	0.928	1.802	−1.541	0.9033	2.556	−1.966
(0.9, 0.1)	0.936	1.807	−1.675	0.9035	2.572	−1.963

$$\sum_{i=1}^{NI} fu_i^{t^{(\cdot)}} + \underbrace{\underbrace{\sum_{s=1}^{NS} UP_s^{t^{(\cdot)}}}_{\text{SPRP}} - p_{\text{ESS}}^{t^{(\cdot)}}}_{\text{Combined Ramping Reserve}} \geqslant URR_{t^{(\cdot)}}, \quad \forall\, i, \forall\, t^{(\cdot)} \tag{35}$$

where $p_{\text{ESS}}^{t^{(\cdot)}}$ is the charged power of ESS at time $t^{(\cdot)}$. By using ESS, power system operators can control the ramping reserves provided by SPRP, and divide it into two parts. One part is to provide ramping reserves for the system, and the other part is to charge the ESS.

6. Conclusion

This paper developed a method to estimate the ramping requirements in multi-timescale power system operations. Considering the rapid increase of solar power in the electric grid, a solar power ramping product (SPRP) was also developed and integrated in the multi-timescale power system operations. A surrogate-based optimization model was used to analytically approximate the multi-objective function considering both economic and reliability benefits of the system. The IEEE 118-bus model was modified to validate the effectiveness of the developed ramping requirements estimation method. Case studies were performed to study: (i) the simulation results of the ramping requirements estimation method; (ii) the accuracy of the surrogate-based optimization model; (iii) the impacts of different standard deviation values of netload under the estimated ramping requirements; and (iv) the impacts of the SPRP under the estimated ramping requirements. Numerical simulations of these case studies showed:

(i) The estimated ramping requirements were accurate through Monte-Carlo simulations and able to successfully capture the preference of balancing authorities.

Table 5
Results of estimated ramping requirements with and without 95% confidence levels.

	Optimal times of standard deviation	Realized conf. level [%]	Prod. cost [$M]
W/o 95% conf. level	α_{opt} = 0.69 β_{opt} = 1.26	50.98 79.24	1.06
With 95% conf. level	α_{opt} = 2.11 β_{opt} = 2.44	96.52 98.54	1.48

(ii) Though both AACEE and σ_{ACE} increased with the standard deviation of netload, there were more economic benefits to the power system due to the use of optimal ramping requirements.
(iii) SPRP played an important role in designing ramping requirements of the real-time unit commitment model, and in the reliability benefits of the power system operation.
(iv) The total ramping reserves in different forecasting scenarios for actual ramps were generally not sufficiently scheduled compared with the perfect forecast, since SPRPs were overestimated by forecasts.

The developed method can be further used in real power system operations. First, the times of standard deviation can be generated and put into the real power system model to calculate both economic and reliability metrics. Second, the multi-objective function can be calculated by these metrics and approximated by the surrogate-based optimization model to find the optimal times of standard deviation. Finally, the estimated ramping reserve requirements of the system can be determined.

In the future, this research could be further improved by: (i) estimating the ramping requirements based on a more accurate probability distribution for the uncertain netload; (ii) comparing both the economic and reliability benefits of SPRP to those of the conventional thermal generator ramping reserve, wind power ramping product, and energy storage ramping product in power system operations; and (iii) studying the impact of the uncertainty and variability of probabilistic solar power ramping products on power system operations.

Acknowledgment

This work was supported by the National Renewable Energy Laboratory under Subcontract No. XGJ-6-62183-01 (under the U.S. Department of Energy Prime Contract No. DE-AC36-08GO28308). The authors would also like to thank the anonymous reviewers for their constructive suggestions to this research.

Appendix A. Gradient and Hessian matrix of the Kriging approximation model

The gradient of the Kriging approximation (KA) model with two variables, α and β, is formulated as:

$$\frac{\partial \hat{f}(\alpha,\beta)}{\partial \alpha} = \frac{\partial \mathscr{F}(\lambda;\alpha,\beta)}{\partial \alpha} + \frac{\partial \mathscr{R}(\omega;\alpha,\beta)}{\partial \alpha} = \frac{\lambda_2}{\sigma_\alpha} + \frac{2\lambda_4(\alpha-\mu_\alpha)}{\sigma_\alpha^2} + \frac{\lambda_5(\beta-\mu_\beta)}{\sigma_\alpha\sigma_\beta} + \frac{2\theta_\alpha}{\sigma_\alpha^2}\sum_{q=1}^{Ns}\omega_q(\alpha_q-\alpha)e^{-\left[\frac{\theta_\alpha(\alpha-\alpha_q)^2}{\sigma_\alpha^2}+\frac{\theta_\beta(\beta-\beta_q)^2}{\sigma_\beta^2}\right]}$$

$$\frac{\partial \hat{f}(\alpha,\beta)}{\partial \beta} = \frac{\partial \mathscr{F}(\lambda;\alpha,\beta)}{\partial \beta} + \frac{\partial \mathscr{R}(\omega;\alpha,\beta)}{\partial \beta} = \frac{\lambda_3}{\sigma_\beta} + \frac{\lambda_5(\alpha-\mu_\alpha)}{\sigma_\alpha\sigma_\beta} + \frac{2\lambda_6(\beta-\mu_\beta)}{\sigma_\beta^2} + \frac{2\theta_\beta}{\sigma_\beta^2}\sum_{q=1}^{Ns}\omega_q(\beta_q-\beta)e^{-\left[\frac{\theta_\alpha(\alpha-\alpha_q)^2}{\sigma_\alpha^2}+\frac{\theta_\beta(\beta-\beta_q)^2}{\sigma_\beta^2}\right]}$$

Components of the Hessian matrix of the KA model, $H(\hat{f}(\alpha,\beta))$, are second partial derivatives and deduced as:

$$\frac{\partial^2 \hat{f}(\alpha,\beta)}{\partial \alpha^2} = \frac{2\lambda_4}{\sigma_\alpha^2} - \frac{2\theta_\alpha}{\sigma_\alpha^2}\sum_{q=1}^{Ns}\omega_q e^{-\left[\frac{\theta_\alpha(\alpha-\alpha_q)^2}{\sigma_\alpha^2}+\frac{\theta_\beta(\beta-\beta_q)^2}{\sigma_\beta^2}\right]} + \frac{4\theta_\alpha^2}{\sigma_\alpha^4}\sum_{q=1}^{Ns}\omega_q(\alpha_q-\alpha)^2 e^{-\left[\frac{\theta_\alpha(\alpha-\alpha_q)^2}{\sigma_\alpha^2}+\frac{\theta_\beta(\beta-\beta_q)^2}{\sigma_\beta^2}\right]}$$

$$\frac{\partial^2 \hat{f}(\alpha,\beta)}{\partial \beta^2} = \frac{2\lambda_6}{\sigma_\beta^2} - \frac{2\theta_\beta}{\sigma_\beta^2}\sum_{q=1}^{Ns}\omega_q e^{-\left[\frac{\theta_\alpha(\alpha-\alpha_q)^2}{\sigma_\alpha^2}+\frac{\theta_\beta(\beta-\beta_q)^2}{\sigma_\beta^2}\right]} + \frac{4\theta_\beta^2}{\sigma_\beta^4}\sum_{q=1}^{Ns}\omega_q(\beta_q-\beta)^2 e^{-\left[\frac{\theta_\alpha(\alpha-\alpha_q)^2}{\sigma_\alpha^2}+\frac{\theta_\beta(\beta-\beta_q)^2}{\sigma_\beta^2}\right]}$$

$$\frac{\partial^2 \hat{f}(\alpha,\beta)}{\partial \alpha\beta} = \frac{\partial^2 \hat{f}(\alpha,\beta)}{\partial \beta\alpha} = \frac{\lambda_5}{\sigma_\alpha\sigma_\beta} + \frac{4\theta_\alpha\theta_\beta}{\sigma_\alpha^2\sigma_\beta^2}\sum_{q=1}^{Ns}\omega_q(\alpha_q-\alpha)(\beta_q-\beta)e^{-\left[\frac{\theta_\alpha(\alpha-\alpha_q)^2}{\sigma_\alpha^2}+\frac{\theta_\beta(\beta-\beta_q)^2}{\sigma_\beta^2}\right]}$$

References

[1] Feng C, Cui M, Hodge B-M, Zhang J. A data-driven multi-model methodology with deep feature selection for short-term wind forecasting. Appl Energy 2017;190:1245–57. http://dx.doi.org/10.1016/j.apenergy.2017.01.043.

[2] Jiang H, Zhang Y, Zhang JJ, Gao DW, Muljadi E. Synchrophasor-based auxiliary controller to enhance the voltage stability of a distribution system with high renewable energy penetration. IEEE Trans Smart Grid 2015;6(4):2107–15. http://dx.doi.org/10.1109/tsg.2014.2387012.

[3] Zhao H, Wu Q, Hu S, Xu H, Rasmussen CN. Review of energy storage system for wind power integration support. Appl Energy 2015;137:545–53. http://dx.doi.org/10.1016/j.apenergy.2014.04.103.

[4] Alam M, Muttaqi K, Sutanto D. A novel approach for ramp-rate control of solar PV using energy storage to mitigate output fluctuations caused by cloud passing. IEEE Trans Energy Convers 2014;29(2):507–18. http://dx.doi.org/10.1109/tec.2014.2304951.

[5] Wang Q, Wu H, Florita AR, Martinez-Anido CB, Hodge B-M. The value of improved wind power forecasting: grid flexibility quantification, ramp capability analysis, and impacts of electricity market operation timescales. Appl Energy 2016;184:696–713. http://dx.doi.org/10.1016/j.apenergy.2016.11.016.

[6] Xu L, Tretheway D. Flexible ramping products. CAISO Proposal; 2014.

[7] Navid N, Rosenwald G. Ramp capability product design for MISO markets. White paper, July; 2013.

[8] Pavić I, Capuder T, Kuzle I. Value of flexible electric vehicles in providing spinning reserve services. Appl Energy 2015;157:60–74. http://dx.doi.org/10.1016/j.apenergy.2015.07.070.

[9] Wang J, Zhong H, Tang W, Rajagopal R, Xia Q, Kang C, et al. Optimal bidding strategy for microgrids in joint energy and ancillary service markets considering flexible ramping products. Appl Energy 2017;205:294–303. http://dx.doi.org/10.1016/j.apenergy.2017.07.047.

[10] Chen R, Wang J, Botterud A, Sun H. Wind power providing flexible ramp product. IEEE Trans Power Syst 2017;32(3):2049–61. http://dx.doi.org/10.1109/tpwrs.2016.2603225.

[11] Cui M, Zhang J, Wu H, Hodge B-M. Wind-friendly flexible ramping product design in multi-timescale power system operations. IEEE Trans Sustain Energy 2017;8(3):1064–75. http://dx.doi.org/10.1109/tste.2017.2647781.

[12] Janko SA, Arnold MR, Johnson NG. Implications of high-penetration renewables for ratepayers and utilities in the residential solar photovoltaic (PV) market. Appl Energy 2016;180:37–51. http://dx.doi.org/10.1016/j.apenergy.2016.07.041.

[13] Li G, Bie Z, Kou Y, Jiang J, Bettinelli M. Reliability evaluation of integrated energy systems based on smart agent communication. Appl Energy 2016;167:397–406. http://dx.doi.org/10.1016/j.apenergy.2015.11.033.

[14] Wang C, Luh P B-S, Navid N. Ramp requirement design for reliable and efficient integration of renewable energy. IEEE Trans Power Syst 2017;32(1):562–71. http://dx.doi.org/10.1109/tpwrs.2016.2555855.

[15] Wang Q, Hodge B-M. Enhancing power system operational flexibility with flexible ramping products: a review. IEEE Trans Indust Inform 2017;13(4):1652–64. http://dx.doi.org/10.1109/tii.2016.2637879.

[16] Ela E, O'Malley M. Studying the variability and uncertainty impacts of variable generation at multiple timescales. IEEE Trans Power Syst 2012;27(3):1324–33. http://dx.doi.org/10.1109/tpwrs.2012.2185816.

[17] Wu H, Krad I, Florita A, Hodge B-M, Ibanez E, Zhang J, et al. Stochastic multi-timescale power system operations with variable wind generation. IEEE Trans Power Syst 2017;32(5):3325–37. http://dx.doi.org/10.1109/tpwrs.2016.2635684.

[18] He M, Murugesan S, Zhang J. A multi-timescale scheduling approach for stochastic reliability in smart grids with wind generation and opportunistic demand. IEEE Trans Smart Grid 2013;4(1):521–9. http://dx.doi.org/10.1109/tsg.2012.2237421.

[19] Flexible Energy Scheduling Tool for Integrating Variable Generation (FESTIV) Model < http://www.nrel.gov/electricity/transmission/festiv.html > .

[20] Welsch M, Deane P, Howells M, Gallachóir BÓ, Rogan F, Bazilian M, et al. Incorporating flexibility requirements into long-term energy system models: a case study on high levels of renewable electricity penetration in Ireland. Appl Energy 2014;135:600–15. http://dx.doi.org/10.1016/j.apenergy.2014.08.072.

[21] Cui M, Zhang J, Wu H, Hodge B-M, Ke D, Sun Y. Wind power ramping product for increasing power system flexibility. In: 2016 IEEE/PES transmission and distribution conference and exposition (T&D). IEEE; 2016, doi:http://dx.doi.org/10.1109/tdc.2016.7520002.

[22] Cui M, Zhang J, Florita A, Hodge B-M, Ke D, Sun Y. Solar power ramp events detection using an optimized swinging door algorithm. In: Volume 2A: 41st design automation conference. ASME; 2015, doi:http://dx.doi.org/10.1115/detc2015-46849.

[23] Cui M, Zhang J, Florita AR, Hodge B-M, Ke D, Sun Y. An optimized swinging door algorithm for identifying wind ramping events. IEEE Trans Sustain Energy 2016;7(1):150–62. http://dx.doi.org/10.1109/tste.2015.2477244.

[24] Zhang J, Florita A, Hodge B-M, Freedman J. Ramp forecasting performance from improved short-term wind power forecasting. In: Volume 2A: 40th design automation conference. ASME; 2014, doi:http://dx.doi.org/10.1115/detc2014-34775.

[25] Kamath C. Associating weather conditions with ramp events in wind power generation. In: 2011 IEEE/PES power systems conference and exposition. IEEE; 2011, doi:http://dx.doi.org/10.1109/psce.2011.5772527.

[26] Cui M, Zhang J, Feng C, Florita AR, Sun Y, Hodge B-M. Characterizing and analyzing ramping events in wind power, solar power, load, and netload. Renew Energy 2017;111:227–44. http://dx.doi.org/10.1016/j.renene.2017.04.005.

[27] Yang Y, Wang J, Guan X, Zhai Q. Subhourly unit commitment with feasible energy delivery constraints. Appl Energy 2012;96:245–52. http://dx.doi.org/10.1016/j.apenergy.2011.11.008.

[28] Wang C, Luh PB, Gribik P, Peng T, Zhang L. Commitment cost allocation of fast-start units for approximate extended locational marginal prices. IEEE Trans Power Syst 2016;31(6):4176–84. http://dx.doi.org/10.1109/tpwrs.2016.2524203.

[29] Ela E, Gevorgian V, Tuohy A, Kirby B, Milligan M, O'Malley M. Market designs for the primary frequency response ancillary service–part I: motivation and design. IEEE Trans Power Syst 2014;29(1):421–31. http://dx.doi.org/10.1109/tpwrs.2013.2264942.

[30] Chaudhry N, Hughes L. Forecasting the reliability of wind-energy systems: a new approach using the RL technique. Appl Energy 2012;96:422–30. http://dx.doi.org/10.1016/j.apenergy.2012.02.076.

[31] North American Electric Reliability Corporation, Reliability standards for the bulk electric systems of North America; 2017 < http://www.nerc.com/pa/Stand/Reliability%20Standards%20Complete%20Set/RSCompleteSet.pdf > .

[32] Ela E, Milligan M, O'Malley M. A flexible power system operations simulation model for assessing wind integration. In: 2011 IEEE power and energy society general meeting. IEEE; 2011, doi:http://dx.doi.org/10.1109/pes.2011.6039033.

[33] Wang Q, Martinez-Anido CB, Wu H, Florita AR, Hodge B-M. Quantifying the

economic and grid reliability impacts of improved wind power forecasting. IEEE Trans Sustain Energy 2016;7(4):1525–37. http://dx.doi.org/10.1109/tste.2016.2560628.
[34] Huang Z, Wang C, Chen J, Tian H. Optimal design of aeroengine turbine disc based on kriging surrogate models. Comp Struct 2011;89(1–2):27–37. http://dx.doi.org/10.1016/j.compstruc.2010.07.010.
[35] Song X, Zhang J, Kang S, Ma M, Ji B, Cao W, et al. Surrogate-based analysis and optimization for the design of heat sinks with jet impingement. IEEE Trans Compon, Pack Manuf Technol 2014;4(3):429–37. http://dx.doi.org/10.1109/tcpmt.2013.2285812.
[36] Gao H, Guo X, Ouyang H, Han F. Crack identification of cantilever plates based on a kriging surrogate model. J Vib Acoust 2013;135(5):051012. http://dx.doi.org/10.1115/1.4023813.
[37] Xia B, Ren Z, Koh C-S. Utilizing kriging surrogate models for multi-objective robust optimization of electromagnetic devices. IEEE Trans Magnet 2014;50(2):693–6. http://dx.doi.org/10.1109/tmag.2013.2284925.
[38] Zhang J, Chowdhury S, Messac A. An adaptive hybrid surrogate model. Struct Multidisc Optim 2012;46(2):223–38. http://dx.doi.org/10.1007/s00158-012-0764-x.
[39] Sacks J, Welch WJ, Mitchell TJ, Wynn HP. Design and analysis of computer experiments. Statist Sci 1989;4(4):409–35.
[40] Wu H, Shahidehpour M, Alabdulwahab A, Abusorrah A. A game theoretic approach to risk-based optimal bidding strategies for electric vehicle aggregators in electricity markets with variable wind energy resources. IEEE Trans Sustain Energy 2016;7(1):374–85. http://dx.doi.org/10.1109/tste.2015.2498200.
[41] DACE < http://www2.imm.dtu.dk/projects/dace > .
[42] GAMS/SCENRED Documentation < http://www.gams.com/help/index.jsp > .
[43] ILOG CPLEX. ILOG CPLEX Homepage 2014 < http://www.ilog.com > .
[44] Shahidehpour M, Yamin H, Li Z. Market operations in electric power systems. New York (NY, USA): Wiley; 2002.
[45] Wu H, Shahidehpour M, Li Z, Tian W. Chance-constrained day-ahead scheduling in stochastic power system operation. IEEE Trans Power Syst 2014;29(4):1583–91. http://dx.doi.org/10.1109/tpwrs.2013.2296438.
[46] IBM. Watt-Sun: a multi-scale, multi-model, machine-learning solar forecasting technology < http://energy.gov/eere/sunshot/watt-sun-multi-scale-multi-model-machine-learning-solar-forecasting-technology > .
[47] Wilcox S, Andreas A. Solar resource & meteorological assessment project (SOLRMAP): Rotating Shadowband Radiometer (RSR) < http://www.nrel.gov/midc/kalaeloa_oahu/ > .
[48] PV Performance Modeling Collaborative (PVPMC). PV_LIB Toolbox < https://pvpmc.sandia.gov/applications/pv_lib-toolbox > .
[49] 66-95-99.7 rule < https://en.wikipedia.org/wiki/68%E2%80%9395%E2%80%9399.7_rule > .